

# Estimation of finite-frequency waveforms through wavelength-dependent averaging of velocity

Anthony Lomax and Roel Snieder

Department of Geophysics, Utrecht University, PO Box 80.021, 3508 TA Utrecht, the Netherlands

Accepted 1996 March 11. Received 1996 March 8; in original form 1996 January 4

## SUMMARY

The wavelength-smoothing (WS) method was introduced recently (Lomax 1994) as a method for the rapid estimation of the principal features of broad-band wave phenomena in realistic, complicated structures. The WS method is based on the concept that waves at a particular frequency and corresponding wavelength respond to a complicated velocity distribution as if the distribution were smoothed over about a wavelength. This method reproduces several finite-frequency wave phenomena, but has not been given a formal theoretical justification. Here, we use scattering theory and a local, plane-wave approximation to develop a wavelength-averaging (WA) method for modelling finite-frequency wave propagation. The new WA method is similar to the WS method in concept and implementation, but is valid only in a more limited geometry of velocity heterogeneity. In particular, the new formulation performs well for models with complex, but smoothly varying, velocity variations ('quasi-random' models), but does less well in models with extensive regions of slowly varying velocity that are separated by strong gradients in velocity ('deterministic' models). This limits application of the current formulation of the WA method to predominantly quasi-random structures, although such models may be useful in many problems, particularly for Monte-Carlo-based inversion methods requiring fast forward calculations.

**Key words:** body waves, inhomogeneous media, synthetic seismograms, wave propagation.

## 1 INTRODUCTION

The wavelength-smoothing method was introduced recently (Lomax 1994) as a method for approximating broad-band wave propagation in complicated velocity structures. This method was developed as an alternative to (1) ray-based methods, which are rapid but only valid for a high-frequency wavefield, (2) waveform methods such as generalized-ray, reflectivity and modal summation techniques, which are efficient and accurate but are only applicable to a limited class of relatively simple structures such as plane layer models, and (3) numerical methods such as finite differences and finite elements, which are applicable to broad-band wave propagation in relatively complicated models but require large computation times. Although not as complete as these existing methods, the wavelength-smoothing method is intended for rapid estimation of the principal features of broad-band wave phenomena in realistic, complicated structures. Such a method is useful for inversion using trial and error, Monte Carlo, and directed search methods such as the genetic algorithm and simulated annealing.

The wavelength-smoothing (WS) method is based on

two principal assumptions (Lomax 1994). First, it is assumed that many features of broad-band wave propagation can be modelled by using Huygens' principle to track the motion of *narrow-band wavefronts* at a number of centre frequencies. Second, it is assumed that the velocity of propagation of body waves at a particular frequency and location can be approximated by a *wavelength-averaged velocity*, given by a centrally weighted average of the medium velocity across the narrow-band wavefront, where the width of the weighting function varies in proportion to the wavelength (Fig. 1). The motion through time of the narrow-band wavefronts determines *wave paths*, which are similar to the rays of ray theory, but are frequency-dependent. The wavelength-dependent smoothing of the medium in the WS algorithm leads to increased stability of the wave paths relative to high-frequency, ray-theory rays and it causes the wave paths to be sensitive to velocity variations within about a wavelength of the wave path (Fig. 2). After many sets of wave paths at a range of centre frequencies have been generated, broad-band waveforms are produced by a summation of the contributions of all wave types at all frequencies arriving at a given receiver location.

The WS method was shown in Lomax (1994) to reproduce

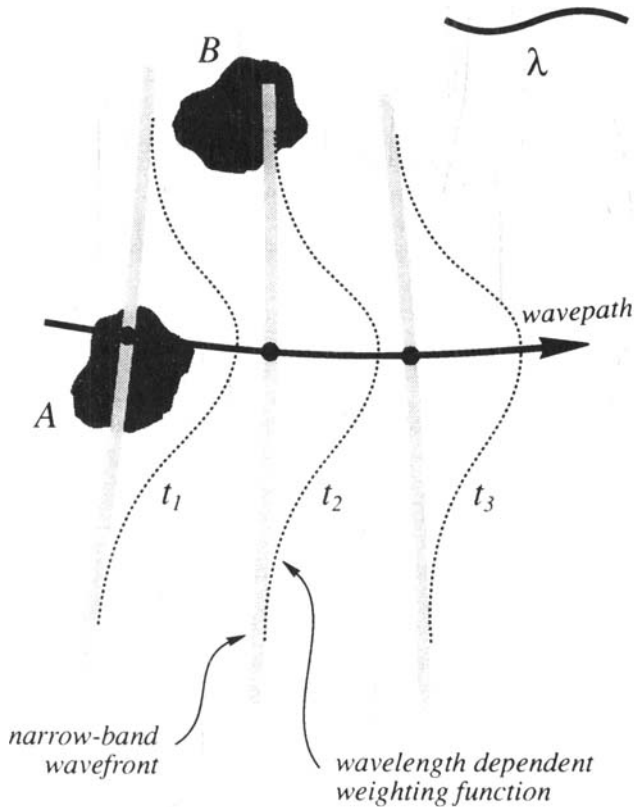


**Figure 1.** Conceptual diagram showing wave path, wavefront and wavelength-dependent weighting function for the wavelength-smoothing method of Lomax (1994). The bell-shaped weighting function is used to smooth the local medium velocity over the wavefront; the smoothed velocity is used to determine the wave path. The propagation is influenced more strongly by velocity variations near the wave path (A) than by those far away (B) relative to the wavelength  $\lambda$ .

many finite-frequency wave phenomena, but was not given a formal theoretical justification. Here, we present a theoretical development that leads to a formulation that is similar to the WS method. We consider an acoustic case with velocity variation in two dimensions. We assume that locally the wave propagation at a single frequency over a small time interval can be represented by plane waves at the beginning and at the end of the interval. Furthermore, we assume that the plane wave at the end of the interval is given by the combination of the first (reference) plane wave and the (Born) scattering of this wave by velocity variations in the (thin) sheet swept out by the reference wave in the (small) time interval. Using this construction, we can track the propagation of many 'wave paths' from the source at distinct frequencies, and construct a broad-band seismogram by combining the results for many frequencies for wave paths passing near the receiver location. Because the estimation of scattering caused by the velocity variation in the thin sheet leads to weighted integrals of velocity perturbation which scale with frequency, we refer to this algorithm as the wavelength-averaging (WA) method.

The resulting WA method is applicable only with some limitations on the scale-length and geometry of the velocity heterogeneity. This new formulation, however, rapidly produces useful synthetics for quasi-random models with strong velocity variations with scale-lengths larger than the dominant wavelength of the source.

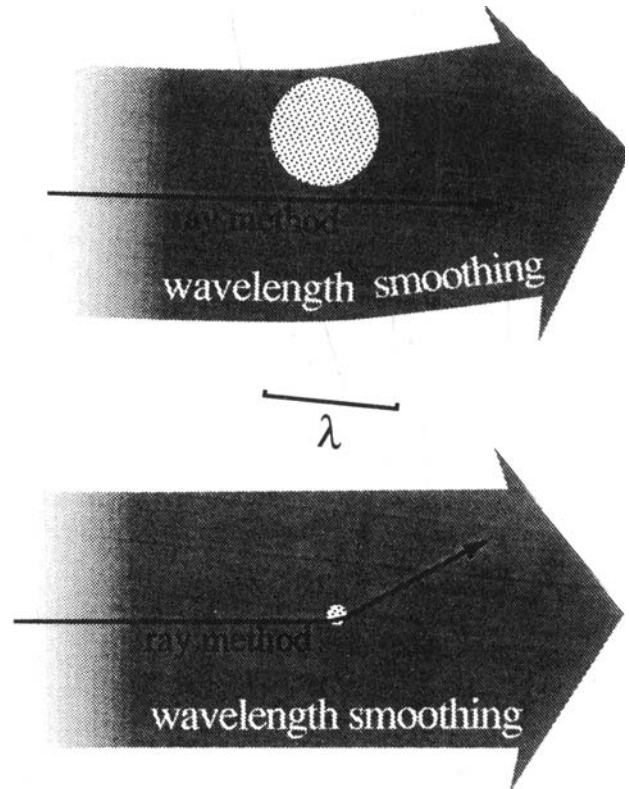


**Figure 2.** Conceptual diagrams showing significant differences between the WS and ray methods. (Top) A ray-theory ray is unperturbed in passing near a velocity anomaly (stippled region), while a WS wave path for wavelength  $\lambda$  will be deflected by an anomaly which is large and close to the wave path relative to  $\lambda$ . (Bottom) A ray-theory ray can be strongly scattered by a small velocity anomaly (stippled region), while a WS wave path for wavelength  $\lambda$  will not be deflected by an anomalous region that is small relative to  $\lambda$ .

## 2 THEORY

The equation of motion in an isotropic, acoustic medium is given by

$$\frac{\partial^2 P}{\partial t^2} = \kappa \frac{\partial}{\partial x_i} \left( \frac{1}{\rho} \frac{\partial P}{\partial x_i} \right), \quad (1)$$

where  $P$  is pressure,  $\kappa$  is incompressibility and  $\rho$  is density. If the density  $\rho$  is constant and only the incompressibility  $\kappa$  varies, then, substituting  $c(\mathbf{r}) = \sqrt{\kappa(\mathbf{r})/\rho}$ , eq. (1) becomes

$$\frac{\partial^2 P}{\partial t^2} = c^2(\mathbf{r}) \nabla^2 P. \quad (2)$$

Using a Fourier transform  $P(\mathbf{r}, t) = \int u(\mathbf{r}, \omega) e^{-i\omega t} d\omega$ , we obtain the Helmholtz equation

$$\nabla^2 u(\mathbf{r}) + \frac{\omega^2}{c^2(\mathbf{r})} u(\mathbf{r}) = 0. \quad (3)$$

### 2.1 Solution by perturbation

Following Snieder & Lomax (1996) and Aki & Richards (1980), we write the velocity field as

$$c(\mathbf{r}) = c_0 + \delta c(\mathbf{r}), \quad (4)$$

where  $c_0$  is a constant 'reference' term and  $\delta c(\mathbf{r})$  a perturbation term. Substituting eq. (4) in eq. (3) we get

$$(c_0^2 + 2c_0\delta c(\mathbf{r}) + [\delta c(\mathbf{r})]^2)\nabla^2 u(\mathbf{r}) + \omega^2 u(\mathbf{r}) = 0. \quad (5)$$

Consider a solution of the form

$$u(\mathbf{r}) = u_0(\mathbf{r}) + u_1(\mathbf{r}), \quad (6)$$

where  $u_0$  is a 'reference' wavefield which is a solution of eq. (3) for the homogeneous medium with constant velocity  $c_0$ ,

$$\nabla^2 u_0(\mathbf{r}) + \frac{\omega^2}{c_0^2} u_0(\mathbf{r}) = 0, \quad (7)$$

and  $u_1$  is a 'scattered' wavefield related to the interaction of  $u_0$  with the velocity perturbation  $\delta c(\mathbf{r})$ . Substituting eq. (6) into eq. (5) and subtracting eq. (7) gives

$$\omega^2 u_1(\mathbf{r}) + c_0^2 \nabla^2 u_1(\mathbf{r}) = -(2c_0\delta c(\mathbf{r}) + [\delta c(\mathbf{r})]^2) \times (\nabla^2 u_0(\mathbf{r}) + \nabla^2 u_1(\mathbf{r})). \quad (8)$$

If we assume that the product of the amplitude and the curvature of the 'scattered' wavefield is small relative to that of the 'reference' wavefield, i.e.

$$|\nabla^2 u_1(\mathbf{r})| \ll |\nabla^2 u_0(\mathbf{r})|, \quad (9)$$

and that the velocity variation is small relative to the reference term,

$$\delta c(\mathbf{r}) \ll c_0, \quad (10)$$

then, neglecting terms in  $\delta c(\mathbf{r}) \cdot \nabla^2 u_1(\mathbf{r})$  and  $[\delta c(\mathbf{r})]^2$  we have

$$\nabla^2 u_1(\mathbf{r}) + \frac{\omega^2}{c_0^2} u_1(\mathbf{r}) = -2 \frac{\delta c(\mathbf{r})}{c_0} \nabla^2 u_0(\mathbf{r}). \quad (11)$$

Eq. (11) is an inhomogeneous wave equation which has a solution

$$u_1(\mathbf{r}_0) = \frac{2\omega^2}{c_0^3} \int_V G(\mathbf{r}_0, \mathbf{r}) \delta c(\mathbf{r}) u_0(\mathbf{r}) dV(\mathbf{r}), \quad (12)$$

where  $G(\mathbf{r}_0, \mathbf{r})$  is the Green's function for eq. (7) with the homogeneous reference medium. This is the Born approximation (Hudson & Heritage 1982) for the field  $u_1(\mathbf{r}_0)$  produced by a single scattering interaction of the reference field  $u_0(\mathbf{r})$  with the velocity perturbation  $\delta c(\mathbf{r})$ .

The Green's function for outgoing waves in a 2-D geometry is (Morse & Feshbach 1953)

$$G(\mathbf{r}_0, \mathbf{r}) = -\frac{i}{4} H_0^{(1)}(\omega r/c_0), \quad (13)$$

where  $r = \sqrt{(z - z_0)^2 + (x - x_0)^2}$  and  $H_0^{(1)}(\omega r/c_0) = J_0(\omega r/c_0) + iY_0(\omega r/c_0)$ . Choosing plane waves travelling in the  $z$ -direction for the reference field,

$$u_0(\mathbf{r}) = A_0 \exp(i\omega(z - z_0)/c_0), \quad (14)$$

and substituting eq. (13), eq. (12) becomes

$$u_1(\mathbf{r}_0) = -\frac{iA_0\omega^2}{2c_0^3} \int_{-\infty}^{\infty} \left\{ \int_{-\infty}^{\infty} H_0^{(1)}(\omega r/c_0) \delta c(\mathbf{r}) \exp(i\omega(z - z_0)/c_0) dx \right\} dz. \quad (15)$$

## 2.2 Thin-slab, local plane-wave approximation

To construct a propagation algorithm for narrow-band paths at frequency  $\omega$  from the preceding theory, we consider the geometry shown in Fig. 3, where all velocity perturbations  $\delta c(\mathbf{r}) = c(\mathbf{r}) - c_0$  are contained within a thin slab  $z_0 - \Delta z < z < z_0$ . In this construction,  $\delta c(\mathbf{r}_0) = 0$  since  $c_0 \equiv c(\mathbf{r}_0)$  is taken as a (local) reference velocity. We approximate the field impinging on the slab in the neighbourhood of  $(x_0, z_0 - \Delta z)$  by a plane-wave reference field  $u_0(\mathbf{r}) = A_0 \exp(i\omega(z - z_0)/c_0)$ ; the orientation of this reference field  $u_0(\mathbf{r})$  determines the orientation of the  $x, z$  coordinate system. A scattered field  $u_1(\mathbf{r})$  due to the interaction of  $u_0(\mathbf{r})$  with the velocity perturbation  $\delta c(\mathbf{r})$  in the thin slab is given by eq. (15). We now assume that the total field  $u_0(\mathbf{r}) + u_1(\mathbf{r})$  in the neighbourhood of  $\mathbf{r}_0$  can be approximated by a new plane wave  $u'(\mathbf{r})$ , with modified amplitude, phase and direction relative to  $u_0(\mathbf{r})$ . This assumption is justified because choosing  $\delta c(\mathbf{r}_0) = 0$  and  $\Delta z$  small relative to the wavelength ensures that the scattered field  $u_1(\mathbf{r})$  will be small relative to  $u_0(\mathbf{r})$ . However, it is possible that for some parts of the narrow-band wavefield this basic assumption will not be accurate; this may occur, for example, where the wave paths touch a caustic of the narrow-band wavefield.

To apply this approximation, we consider a general plane wave  $u'(\mathbf{r})$  propagating in the  $(n_z, \Delta n_x)$ -direction away from the slab with amplitude  $A'$  and phase shift  $\Delta\phi$  as an approximation to the total outgoing field at  $\mathbf{r} = (x, z)$  in the vicinity of  $\mathbf{r}_0 = (x_0, z_0)$ :

$$u'(\mathbf{r}) = A' \exp(i\{\omega[n_z(z - z_0) + \Delta n_x(x - x_0)]/c_0 + \Delta\phi\}), \quad (16)$$

where  $A'$ ,  $\Delta n_x$  and  $\Delta\phi$  are independent of  $\mathbf{r}$ . In this notation we anticipate that  $A' \sim A$ ,  $\Delta n_x \sim 0$  and  $\Delta\phi \sim 0$ . Equating the

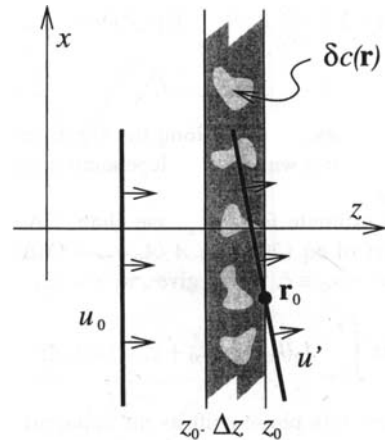


Figure 3. Construction for wavelength-averaging approximation showing a thin region of velocity variation  $\delta c(\mathbf{r})$ , incident plane wave  $u_0$ , and plane-wave approximation to the scattered wavefield  $u'$ . The  $x, z$  coordinate system is determined by the propagation direction of  $u_0$ .

sum of the reference and scattered fields to  $u'(\mathbf{r})$ ,

$$u_0(\mathbf{r}) + u_1(\mathbf{r}) = u'(\mathbf{r}), \quad (17)$$

and substituting eq. (14), (15) and (16), we arrive at

$$\begin{aligned} & A_0 \exp(i\omega(z - z_0)/c_0) - \frac{iA_0\omega^2}{2c_0^3} \int_{z_0 - \Delta z}^{z_0} \\ & \times \left\{ \int_{-\infty}^{\infty} H_0^{(1)}(\omega r(x', z')/c_0) \delta c(x', z') \exp(i\omega(z' - z_0)/c_0) dx' \right\} dz' \\ & = A' \exp(i\{\omega[n_z(z - z_0) + \Delta n_x(x - x_0)]/c_0 + \Delta\varphi\}). \end{aligned} \quad (18)$$

We can choose  $\Delta z$  small and write  $\int_{z_0 - \Delta z}^{z_0} f(z) dz \sim f(z_0)\Delta z$ , and eq. (18) evaluated at  $z = z_0$  becomes

$$\begin{aligned} & A_0 - \frac{iA_0k_0^2\Delta z}{2c_0} \int_{-\infty}^{\infty} H_0^{(1)}(k_0 r(x', z_0)) \delta c(x', z_0) dx' \\ & = A' \exp(i[k_0\Delta n_x(x - x_0) + \Delta\varphi]), \end{aligned} \quad (19)$$

where we have substituted  $k_0 = \omega/c_0$ . Finally, separating the real and imaginary terms in this expression and substituting the first-order Taylor expansion of the exponential on the right-hand side, we obtain

$$\begin{aligned} & A_0 - \frac{iA_0k_0^2\Delta z}{2c_0} \int_{-\infty}^{\infty} J_0(k_0 r(x', z_0)) \delta c(x', z_0) dx' \\ & + \frac{A_0k_0^2\Delta z}{2c_0} \int_{-\infty}^{\infty} Y_0(k_0 r(x', z_0)) \delta c(x', z_0) dx' \\ & \sim A'(1 + ik_0\Delta n_x(x - x_0) + i\Delta\varphi). \end{aligned} \quad (20)$$

The integrals in this equation have the form of weighted averages of velocity perturbation  $\delta c$  along the  $x$ -axis.

### 2.3 Amplitude change, apparent velocity and direction change

To find an estimate for the amplitude change  $A'/A_0$  we take the real part of eq. (20) and substitute  $r|_{z=z_0} = x' - x_0 \equiv \xi$ , which gives, at  $x = x_0$ ,

$$(A'/A_0)(k_0, \mathbf{r}_0) \sim 1 + \frac{k_0}{2c_0} \Delta z \int_{-\infty}^{\infty} Y_0(k_0 \xi) \delta c(x_0 + \xi, z_0) d(k_0 \xi), \quad (21)$$

where  $k_0 \xi$  expresses distance along the  $x$ -axis in radians. This is an expression for a wavelength-dependent amplitude change  $(A'/A_0)(k_0, \mathbf{r}_0)$ .

To find an estimate for the phase change  $\Delta\varphi$  we take the imaginary part of eq. (20), put  $A'/A_0 = 1 + O(\Delta z)$  and substitute  $r|_{z=z_0} = x' - x_0 \equiv \xi$ , which gives, at  $x = x_0$ ,

$$\Delta\varphi \sim -\frac{k_0}{2c_0} \Delta z \int_{-\infty}^{\infty} J_0(k_0 \xi) \delta c(x_0 + \xi, z_0) d(k_0 \xi). \quad (22)$$

We can express this phase shift as an apparent velocity  $\bar{c}$  by writing

$$\exp(i[\omega\Delta z/c_0 + \Delta\varphi]) = \exp(i\omega\Delta z/\bar{c}), \quad (23)$$

which gives

$$\begin{aligned} \bar{c} &= \frac{\omega\Delta z}{\omega\Delta z/c_0 + \Delta\varphi} = c_0 \left( \frac{1}{1 + \frac{c_0\Delta\varphi}{\omega\Delta z}} \right) \sim c_0 \left( 1 - \frac{c_0\Delta\varphi}{\omega\Delta z} \right) \\ &= c_0 \left( 1 - \frac{\Delta\varphi}{k_0\Delta z} \right), \end{aligned} \quad (24)$$

for  $\Delta\varphi \ll 1$ . Substituting from eq. (22) for  $\Delta\varphi$  we obtain

$$\bar{c}(k_0, \mathbf{r}_0) \sim c_0 + \frac{1}{2} \int_{-\infty}^{\infty} J_0(k_0 \xi) \delta c(x_0 + \xi, z_0) d(k_0 \xi), \quad (25)$$

which is an expression for a wavelength-dependent, apparent velocity  $\bar{c}(k_0, \mathbf{r}_0)$ .

To find an estimate for the change in direction  $\Delta n_x$  we differentiate the imaginary part of eq. (20) with respect to  $x$ , and writing  $r|_{z=z_0} = x - x_0 \equiv \xi$  we get, at  $x = x_0$ ,

$$\Delta n_x(k_0, \mathbf{r}_0) \sim \frac{-\Delta z}{2c_0} \frac{\partial}{\partial x} \bigg|_{x_0} \int_{-\infty}^{\infty} J_0(k_0 \xi) \delta c(x_0 + \xi, z_0) d(k_0 \xi), \quad (26)$$

where  $k_0 \xi$  express distance along the  $x$ -axis in radians. This is an expression for a wavelength-dependent direction change  $\Delta n_x(k_0, \mathbf{r}_0)$ . We show later that eqs (25) and (26) are equivalent to the equation of kinematic ray tracing for a medium with velocity  $\bar{c}$ .

## 3 NUMERICAL IMPLEMENTATION

The construction of a numerical propagation algorithm from eqs (21), (25) and (26) requires replacing the averaging integrals from  $-\infty$  to  $\infty$  over  $k_0 \xi$  with sums over a finite interval. In general there will be a truncation error associated with such a replacement. Here we will construct the finite sums so that the error is minimal for: (1) a constant-velocity medium, and (2) velocity perturbations only within the finite interval of the summation over  $k_0 \xi$ . The first case is accounted for by choosing the velocity at  $\mathbf{r}_0 = (x_0, z_0)$  for the reference velocity  $c_0$ , i.e.  $c_0 = c(x_0, z_0)$ . With this choice,  $\delta c(\mathbf{r})$  is everywhere zero in a constant-velocity medium, and consequently  $\bar{c} = c_0$ ,  $\Delta n_x = 0$  and  $A'/A_0 = 1$ . The second case is accounted for if we apply no normalization to the truncated sums. Note, however, that there is in general still a truncation error, for example in the case of velocity variation outside the finite interval of summation.

For the apparent velocity, we substitute  $\theta = k_0 \xi$  and  $x(\theta) = x_0 + \theta/k_0$  in eq. (25) to get

$$\bar{c}(k_0, \mathbf{r}_0) \sim c_0 + \frac{1}{2} \int_{-\infty}^{\infty} J_0(\theta) \delta c(x(\theta), z_0) d\theta. \quad (27)$$

Note that  $\theta$  expresses a phase delay in radians, that  $\theta/2\pi$  gives distance in wavelengths, and that  $x(\theta)$  is dependent on  $k_0$ . We truncate the integral in eq. (27) at  $\pm\theta_{\max}$  and convert it to a sum over  $2M + 1$  terms, giving

$$\bar{c}(k_0, \mathbf{r}_0) \sim c_0 + \bar{s}(k_0, \mathbf{r}_0), \quad (28)$$

where

$$\bar{s}(k_0, \mathbf{r}_0) = \frac{1}{2} \sum_{m=-M}^{m=M} w(\theta_m) \delta c(x(\theta_m), z_0), \quad (29)$$

$$w(\theta_m) = \int_{\theta_m - \Delta\theta/2}^{\theta_m + \Delta\theta/2} J_0(\theta) d\theta, \quad (30)$$

$\Delta\theta = \theta_{\max}/M$ , and  $\theta_m = m\Delta\theta$ . In this construction we have made the assumption that  $\delta c(x(\theta), z_0)$  is slowly varying on any interval  $\theta_m - \Delta\theta/2 \leq \theta \leq \theta_m + \Delta\theta/2$ , so that it does not need to be included inside the integral in eq. (30). This condition restricts the velocity perturbations to be smooth on a scale-length of  $\Delta\theta/k_0$ .

Similarly, for the change in direction  $\Delta n_x$  we obtain

$$\Delta n_x(k_0, \mathbf{r}_0) \sim \frac{-\Delta z}{2c_0} \frac{\partial}{\partial x_0} \bar{s}(k_0, \mathbf{r}_0) \quad (31)$$

from eq. (26). Approximating  $\partial f/\partial x_0$  by

$$\frac{f(x_0 + \Delta\theta/k_0) - f(x_0 - \Delta\theta/k_0)}{2\Delta\theta/k_0},$$

choosing  $\Delta z = c_0\Delta t$  where  $\Delta t$  is the (small) time-step used for calculation, we get

$$\begin{aligned} \Delta n_x(k_0, \mathbf{r}_0) \sim & \frac{\Delta t}{4\Delta\theta/k_0} \\ & \times [\bar{s}(k_0, x_0 + \Delta\theta/k_0, z_0) - \bar{s}(k_0, x_0 - \Delta\theta/k_0, z_0)]. \end{aligned} \quad (32)$$

For the change in amplitude  $A'/A_0$  we substitute  $\theta = k_0\xi$  and  $x(\theta) = x_0 + \theta/k_0$  in eq. (21) to arrive at

$$A'/A_0 \sim 1 + \frac{k_0}{2c_0} \Delta z \int_{-\infty}^{\infty} Y_0(\theta) \delta c(x(\theta), z_0) d\theta. \quad (33)$$

We truncate the integral at  $\pm\theta_{\max}$ , which gives

$$A'/A_0 \sim 1 + \frac{k_0}{2c_0} \Delta z \bar{s}'(k_0, \mathbf{r}_0), \quad (34)$$

where

$$\bar{s}'(k_0, \mathbf{r}_0) = \sum_{m=-M}^{m=M} w'(\theta_m) \delta c(x(\theta_m), z_0), \quad (35)$$

and

$$w'(\theta_m) = \int_{\theta_m - \Delta\theta/2}^{\theta_m + \Delta\theta/2} Y_0(\theta) d\theta. \quad (36)$$

Finally, choosing  $\Delta z = c_0\Delta t$  we get

$$A'/A_0 \sim 1 + \frac{k_0}{2} \Delta t \bar{s}'(k_0, \mathbf{r}_0). \quad (37)$$

The weighting functions developed above,  $w(\theta_m)$  and  $w'(\theta_m)$ , are significantly different in form from the weighting function used in the wavelength-smoothing formulation in Lomax (1994). The weighting function developed by trial and error in the earlier work has the form of a Gaussian bell curve and is real and positive (Fig. 4). The broad and smooth character of this function leads to a stable 'averaging' of the medium properties, but gives no direct amplitude information. The new functions developed here are oscillatory and they form a real and imaginary pair (Fig. 4). The real and imaginary parts relate to the wave-path kinematics and amplitude variation, respectively. However, the relatively narrow, positive-negative oscillations in these functions lead to some instability in rapidly varying structures. For example, the interaction between positive and negative lobes of  $w(\theta_m)$  and a sub-lobe-sized velocity anomaly can lead to an oscillation between nearby wave paths.

The frequency-independent weighting functions  $w(\theta_m)$  and  $w'(\theta_m)$  depend on two parameters,  $\theta_{\max}$  and  $M$ . As  $\theta_{\max}$  is increased, the weighting function is widened and includes more oscillations. This will bring more distant velocity perturbations and corresponding scattering effects into the propagation, but, because the plane-wave approximation will not be valid far from the wave path, choosing  $\theta_{\max}$  very large will not necessarily improve the overall quality of the resulting wavefield estimation. Also, as  $\theta_{\max}$  is increased,  $M$  must also be increased to maintain the precision of the calculation. Here, we choose  $\theta_{\max} \sim 2.5$  wavelengths, and we choose  $M \sim 30$  so that there are several weighting points for each lobe of the weighting function (Fig. 4).

If the scale-length of the velocity variation  $\delta c(\mathbf{r})$  is much greater than the size of the lobes in the WA weighting functions  $w(\theta_m)$  and  $w'(\theta_m)$  (cf. Fig. 4), then the averaging integrals evaluate to nearly zero. Conversely, the largest contribution from these (approximate) functions will occur if the velocity variation occurs on a scale-length similar to or less than the

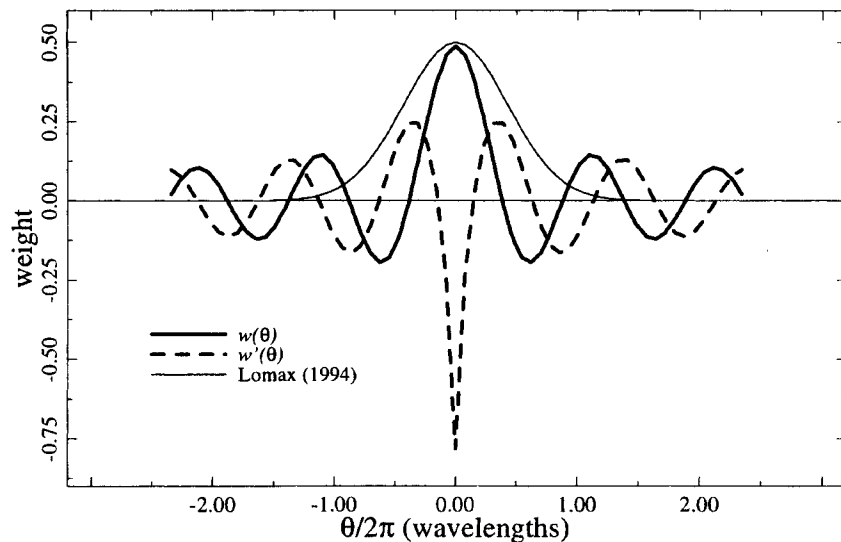


**Figure 4.** Real,  $w(\theta)$ , and imaginary,  $w'(\theta)$ , parts of the WA weighting function derived here and the weighting function from Lomax (1994) for WS plotted as a function of distance in wavelengths along the wavefront from the observation point  $\mathbf{r}_0 = (x_0, z_0)$ . The relative amplitude scaling of the WA and WS weighting functions is not significant.

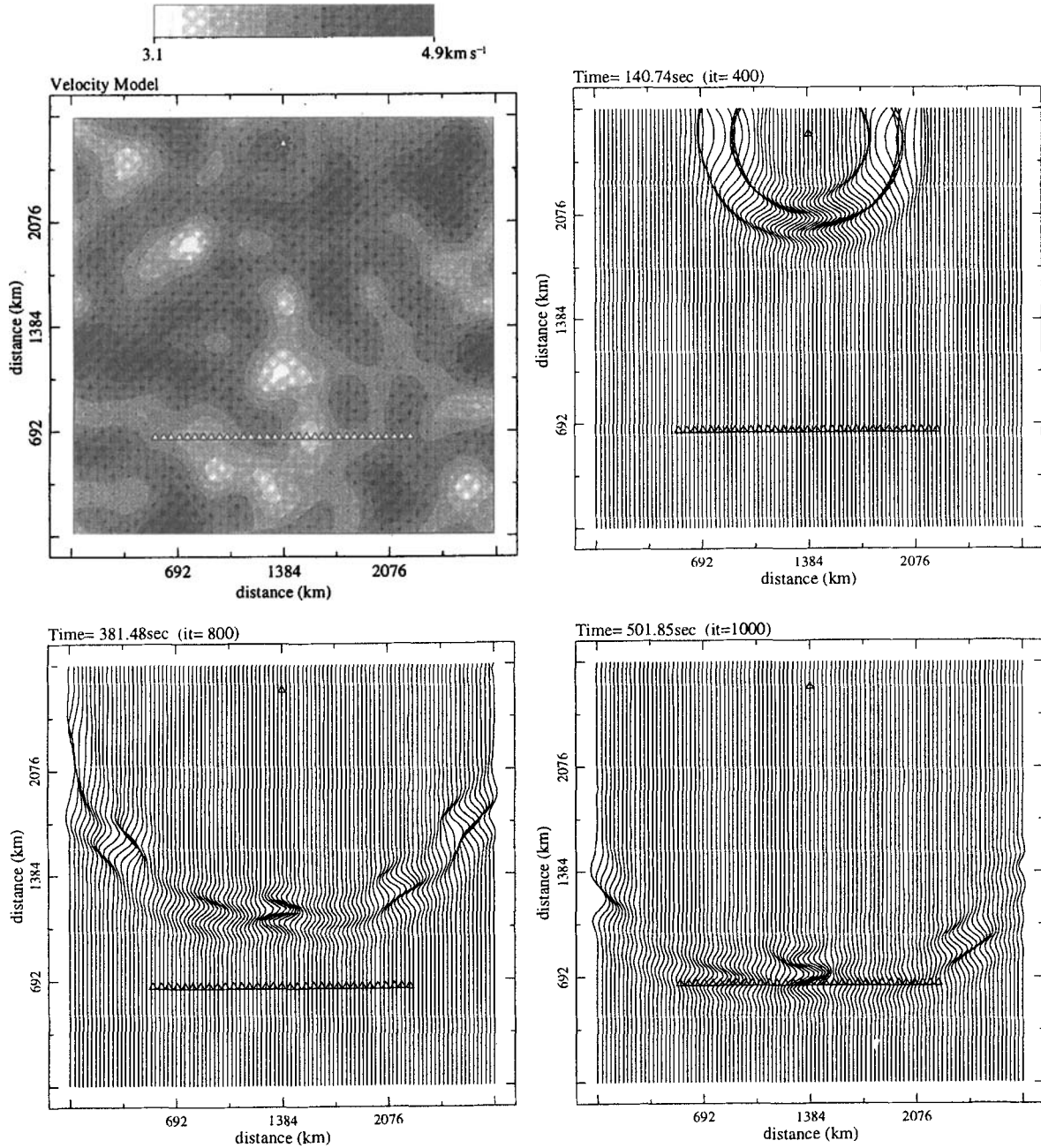


**Figure 5.** Velocity model and finite-difference wavefield for a smooth, 'quasi-random' velocity field and narrow-band source function. The velocity structure is obtained by low-pass filtering a random, normally distributed set of velocity values on a  $512 \times 512$  point grid. The source function has the form  $u(t) = A \exp(-2\pi t/\alpha T_0)^2 \cos(2\pi t/T_0)$ , where  $T_0 = 50$  s and  $\alpha = 5$ . Locations of synthetic seismograms are indicated by triangles.

dominant wavelength of the signal. Since we assumed in eqs (9) and (10) that the scattered field is small relative to the reference field, and since the strength of the scattered field is related to the contribution of the averaging integrals, there is an indication that the velocity variation must be smooth on the scale of a wavelength. This is similar to, but perhaps less severe than, the restrictions for geometrical optics, where the parameters of the medium and the wave should be smooth on a scale-length similar to the width of the Fresnel volume (Kravtsov & Orlov 1993). Other factors, such as the validity of the plane-wave, thin-sheet construction shown in Fig. 3 and the selection of truncation parameters for converting the

averaging integrals to sums, will also affect the accuracy of the results.

### 3.1 Relation with kinematic ray tracing

It can be shown that eq. (25) for the wavelength-dependent velocity  $\bar{c}$  and eq. (26) for the change in direction  $\Delta n_x$  together are equivalent to the equations for ray paths in a medium with local velocity  $\bar{c}$ . Consider the equation of kinematic ray tracing (Aki & Richards 1980),

$$\frac{d}{ds} \left( \frac{1}{c} \frac{dr}{ds} \right) = \nabla \frac{1}{c}, \quad (38)$$

where  $s$  is distance along the ray,  $c$  is velocity and  $\mathbf{r}$  is the location in space. Putting  $d\mathbf{r}/ds \equiv \hat{\mathbf{n}}$  for the unit vector along a ray, and  $\nabla = \hat{\mathbf{n}} d/ds + \nabla_{\perp}$ , where  $\nabla_{\perp}$  is the component of gradient normal to  $\hat{\mathbf{n}}$ , eq. (38) becomes

$$\frac{d}{ds} \left( \frac{1}{c} \right) \hat{\mathbf{n}} + \frac{1}{c} \frac{d}{ds} \hat{\mathbf{n}} = \frac{d}{ds} \left( \frac{1}{c} \right) \hat{\mathbf{n}} + \nabla_{\perp} \left( \frac{1}{c} \right), \quad (39)$$

$$\frac{d\hat{\mathbf{n}}}{ds} = c \nabla_{\perp} \left( \frac{1}{c} \right) = -\frac{1}{c} \nabla_{\perp} c. \quad (40)$$

Eq. (26) for the WA direction change can be rewritten, using eq. (25),

$$\Delta n_x \sim \frac{-\Delta z}{c_0} \frac{\partial \bar{c}}{\partial x}, \quad (41)$$

and since, in terms of ray-centred coordinates, we move our wave location a distance  $\Delta s = \bar{c} \Delta t = \bar{c} \Delta z / c_0$  in one time-step, eq. (41) becomes, in the limit of  $\Delta n_x / \Delta s \rightarrow dn_x / ds$ ,

$$\frac{dn_x}{ds} = -\frac{1}{\bar{c}} \frac{\partial \bar{c}}{\partial x}, \quad (42)$$

which is equivalent to eq. (40). Hence, in a medium with a local velocity  $c$ , the WA method produces finite-frequency wave paths which are identical to the (infinite frequency) ray

paths for a medium with local velocity  $\bar{c}$ . Conversely, this result implies that inferences of velocity structure using ray theory and finite-frequency data can at best only recover an 'averaged' velocity structure related to  $\bar{c}$ .

### 3.2 Construction of seismograms

To construct a synthetic seismogram for receiver  $j$ , eqs (28) and (31) are applied repeatedly at small time increments to trace many wave paths at various take-off angles from a point source. An amplitude change at each time-step is given by eq. (34). The coordinates  $x$  and  $z$  in these equations are defined by the wave-path orientation and will change at each time-step. A different set of wave paths is generated for each of a number of centre frequencies  $f_n$  which cover the band of interest. Arrival times  $t_{j,n}$  and total amplitude change  $A_{j,n}/A_0$  for receiver  $j$  and frequency  $n$  are interpolated from the wave paths that pass closest to the location of the receiver. Additionally, the amplitude is multiplied by a factor  $g_j$  for 2-D ( $1/\sqrt{R}$ ) or 3-D ( $1/R$ ) geometrical spreading, where  $R$  is the distance from the source to the receiver, and the amplitude can be adjusted to reflect a source radiation pattern.

The response at a given station for each arrival at centre frequency  $f_n$  is formed by summing into a time series  $s_n$ , at

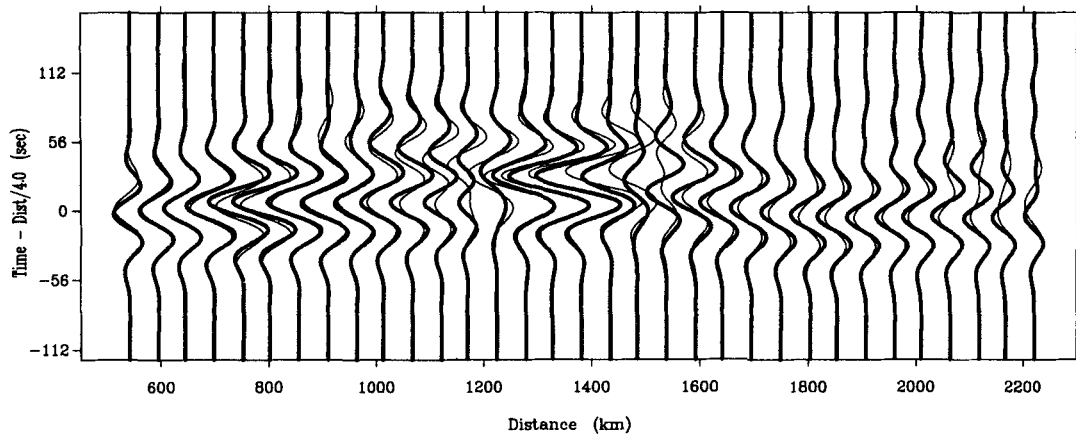


**Figure 6.** Narrow-band source, synthetic FD seismograms (thin lines) and WA seismograms (thick lines) for the 'quasi-random' model and receiver locations shown in Fig. 5.

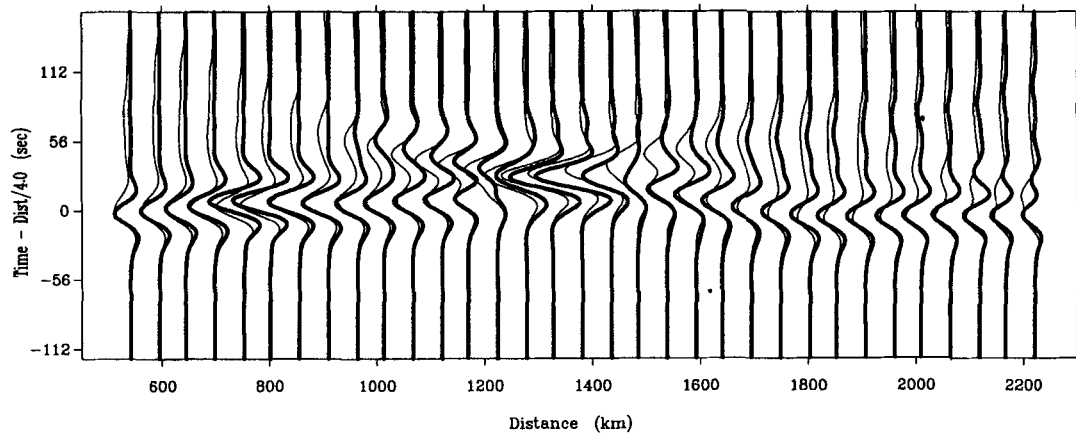


**Figure 7.** Broad-band source ( $T_0 = 50$  s,  $\alpha = 2.5$ ), synthetic FD seismograms (thin lines) and WA seismograms (thick lines) for the 'quasi-random' model and receiver locations shown in Fig. 5.

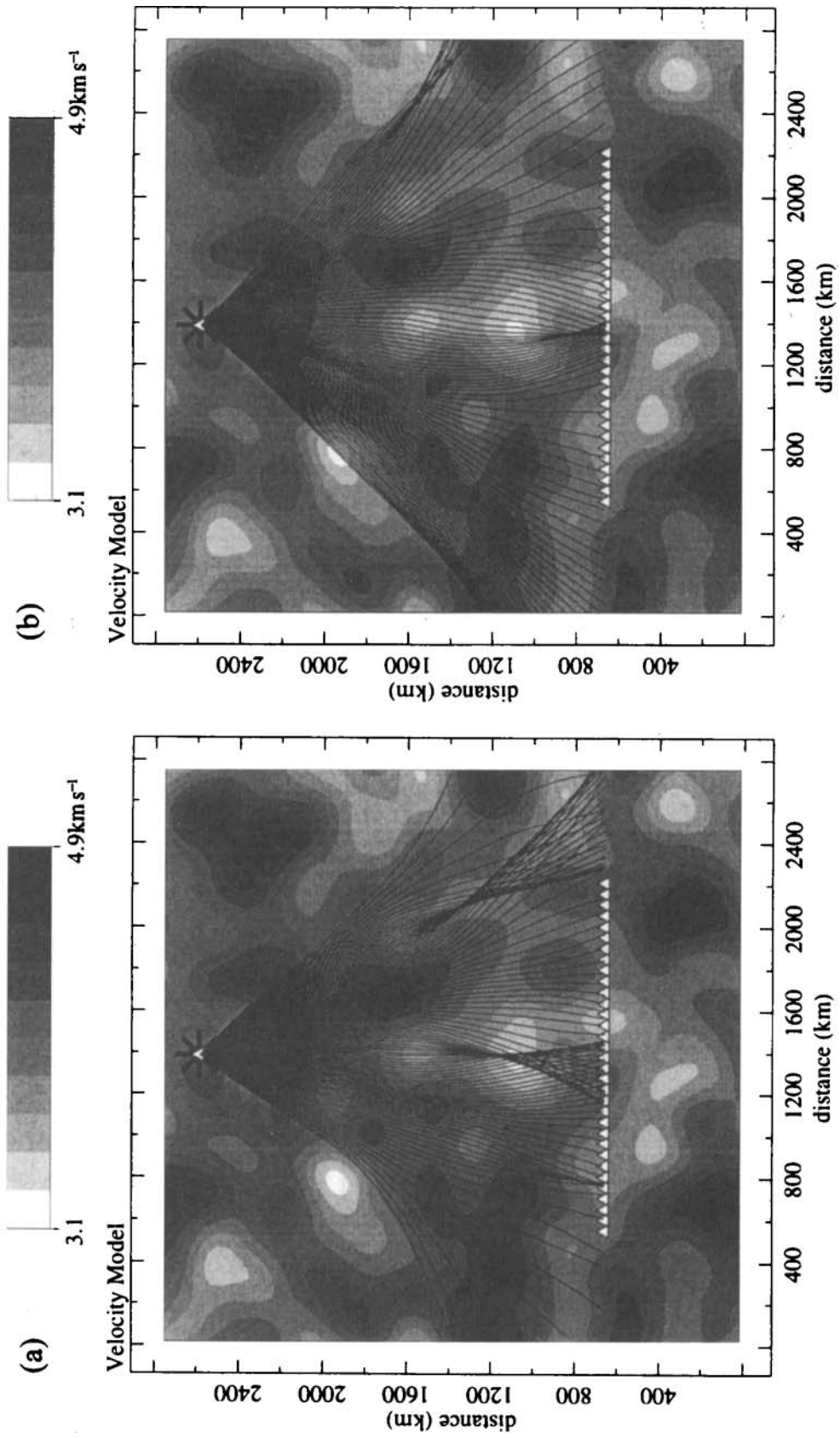


Figure 8. Wavelength-averaging wave paths at (a)  $T_0 = 50$  s and (b)  $T_0 = 200$  s for the 'quasi-random' model in Fig. 5.

arrival time  $t_{j,n}$ , a narrow-band filtered delta function  $\delta_n$  which is scaled by the amplitude change  $A_{j,n}/A_0$  and geometrical spreading  $g_j$ :

$$s_n(t, f_n) = \sum_j \frac{g_j A_{j,n}}{A_0} \delta_n(t - t_{j,n}). \quad (43)$$

The narrow-band delta function  $\delta_n$  is formed by Gaussian filtering a delta function at centre frequency  $f_n$ .

A broad-band time series  $s(t)$  is constructed by summing the narrow-band time series  $s_n$  for each frequency:

$$s(t) = \sum_n s_n(t, f_n). \quad (44)$$

The time series  $s(t)$  approximates the response at a given station to an impulsive source within the frequency band used for the wavelength-averaging wave-path calculations. This band-limited, impulse response time series can be convolved with a source time function to produce a synthetic seismogram.

This procedure differs from the original formulation of Lomax (1994) in that here the amplitude is estimated from a combination of geometrical spreading  $g_j$  due to source–receiver offset, and the cumulative amplitude change  $A_{j,n}/A_0$  given by the application of eq. (37) at each time-step. Previously, the amplitude was estimated from the separation of wave paths near the receiver relative to their separation near the source; this estimate was subject to instability if the separation between adjacent wave paths was small.

#### 4 NUMERICAL EXAMPLES

Through comparison with finite-difference seismograms, we show that the theory developed above gives useful results for models with velocity variations that are smooth on the scale of a wavelength, but not necessarily small in magnitude. We examine two types of model, one with random and relatively smooth velocity variations, referred to here as a ‘quasi-random’ model, and the other with relatively extensive regions of nearly constant velocity separated by relatively strong gradients in velocity, referred to here as a ‘deterministic’ model. A better match of the WA to the finite-difference seismograms is obtained for ‘quasi-random’ than for ‘deterministic’ velocity variations.

##### 4.1 Finite-difference method

We use a finite-difference (FD) algorithm to solve the equation of motion in an isotropic, acoustic medium (eq. 1) for constant density on a 2-D grid. This algorithm is of second order in time and fourth order in space, with transmitting boundary conditions. For the WA calculation, the velocity outside the grid is set equal to the mean velocity within the grid. In general the WA method is up to an order of magnitude faster than the FD method for the same problem, and the WA method requires insignificant memory above that needed for storage of the velocity model.

##### 4.2 Smooth quasi-random models

We first compare the finite-difference and WS results for a narrow-band point source ( $T_0 = 50$  s) in a quasi-random model (Gaussian) which is smooth on length scales smaller than a wavelength, but which has a large velocity variation of  $\pm 20$  per cent. Fig. (5) shows the velocity model and the wave propagation for the finite-difference simulation. Fig. (6) shows finite-difference and WA seismograms for the locations shown in Fig. (5). There is a good overall match between the WA and FD seismograms in phase and amplitude for first- and later-arriving energy. The phase delay and amplitude increase at about  $\Delta \sim 1300$  km and the second-arrival branch at  $900 < \Delta < 1600$  km are significant features of this simulation that are reproduced in the WA calculation. The greatest mismatch in waveforms occurs in regions of wave focusing ( $\Delta \sim 800, 1400$  km) and interference ( $\Delta \sim 1200, 1500, 2100$  km). Given that the WA calculation is about an order of magnitude faster than the FD calculation, these results indicate that the WA calculation gives a useful estimate of the wavefield for this model geometry.

Fig. (7) shows FD and WA synthetics for the velocity model and receiver locations shown in Fig. (5) with a broad-band point source. Again the overall match in phase and amplitude is very good, although there is significant mismatch in the regions of wave interference at about  $\Delta \sim 1100$  and 1500 km. Also, there is a poor match to the longer-period signal between the first- and later-arriving energy (i.e. at  $\Delta < 1000$  km and in

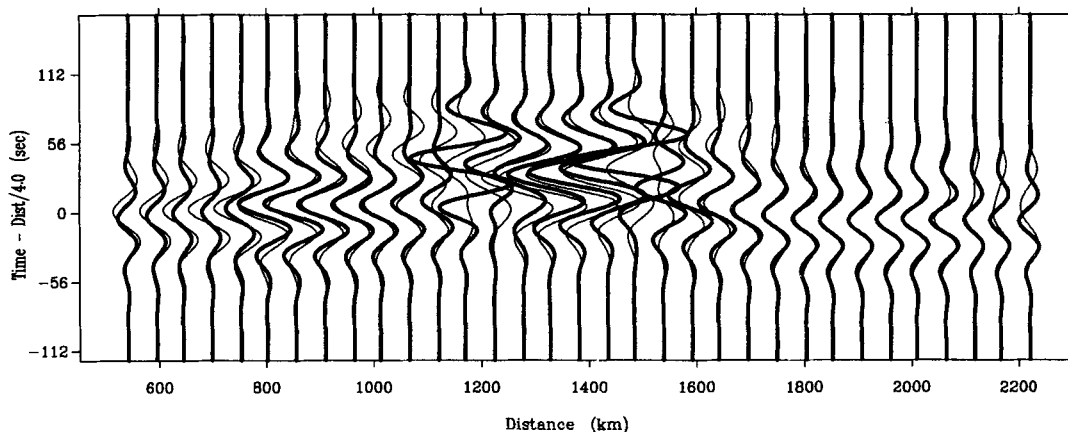
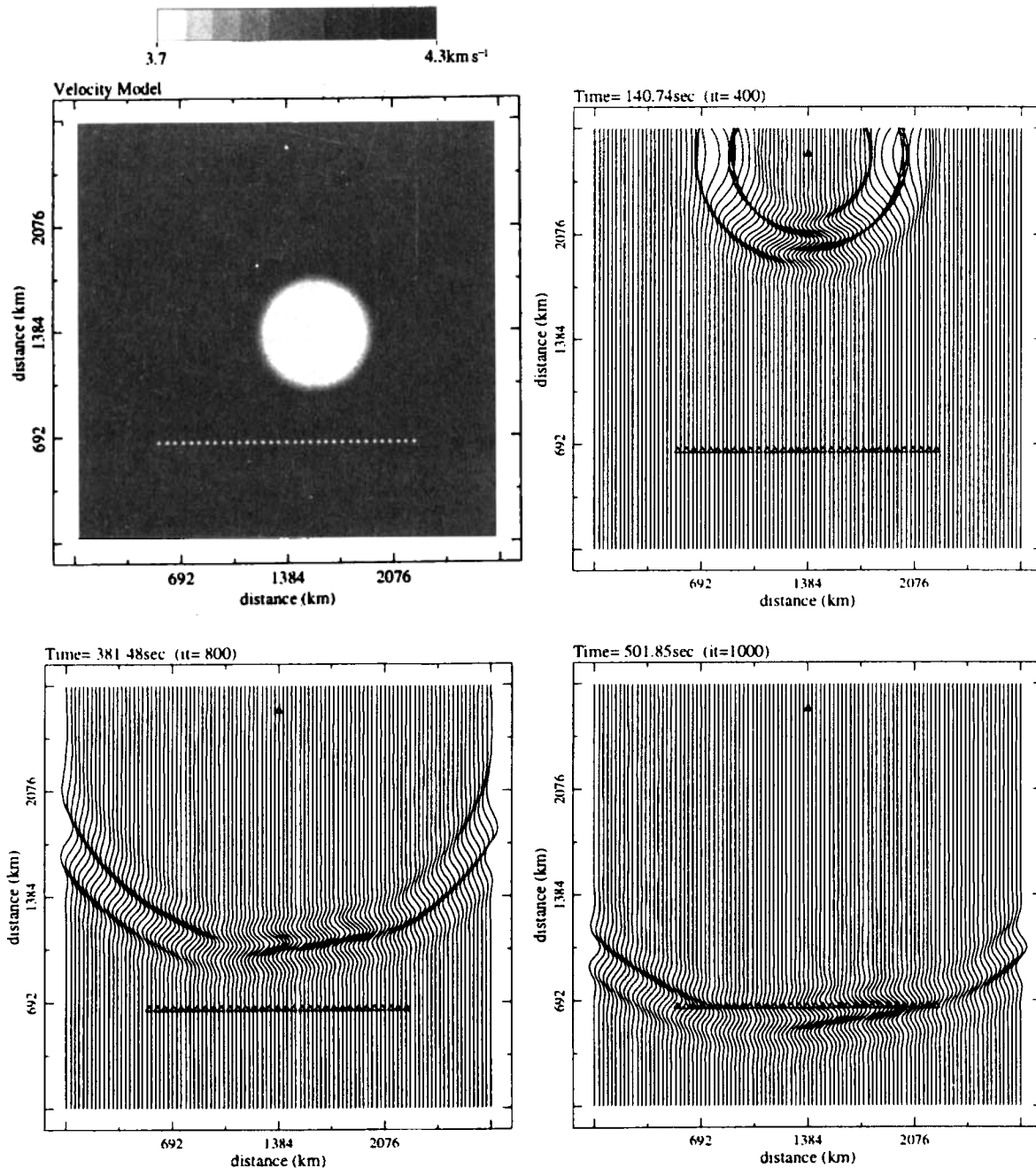


Figure 9. Simple ray-theory synthetic seismograms (thick lines) and FD seismograms (thin lines) for the ‘quasi-random’ model and receiver locations shown in Fig. 5.



**Figure 10.** Velocity model and finite-difference wavefield for a 'deterministic', low-velocity disc, velocity field and narrow-band source function. The source function has the form  $u(t) = A \exp(-(2\pi t/\alpha T_0)^2) \cos(2\pi t/T_0)$ , where  $T_0 = 50$  s and  $\alpha = 5$ . Locations of synthetic seismograms are indicated by triangles.

the range  $1600 < \Delta < 1900$  km). This mismatch may indicate that the velocity variation in the model varies on too small a scale-length for the longest periods in the simulation, and may indicate the presence of a wave phenomenon, such as diffraction, that is not well modelled by the WA algorithm. The comparison at longest periods may also be affected by the difference in the treatments of the boundary of the grid in the WA and FD algorithms.

In Fig. (8) we show some of the WA wave paths for periods of 50 and 200 s for the quasi-random model. The wave paths at 50 s are similar to ray-theory ray paths for this model, but are slightly smoother due to the averaging of the medium in

the WA method. The WA wave paths for longer periods (*cf.* Fig. 8b) produce a smoother wavefield, while those at shorter periods are nearly identical to the ray-theory ray paths. However, the synthetics obtained from simple ray theory are very different from the WA synthetics. In Fig. (9) we show ray synthetics using a simple amplitude estimate based on the separation between ray paths. These ray synthetics show significant amplitude instability at the caustics in the ray field near  $\Delta = 800, 1150, 1500$  km which do not appear in the WA synthetics (Fig. 6). This comparison shows that the WA method is not subject to some of the instabilities in critical regions that occur with simple ray theory. The WA synthetics also

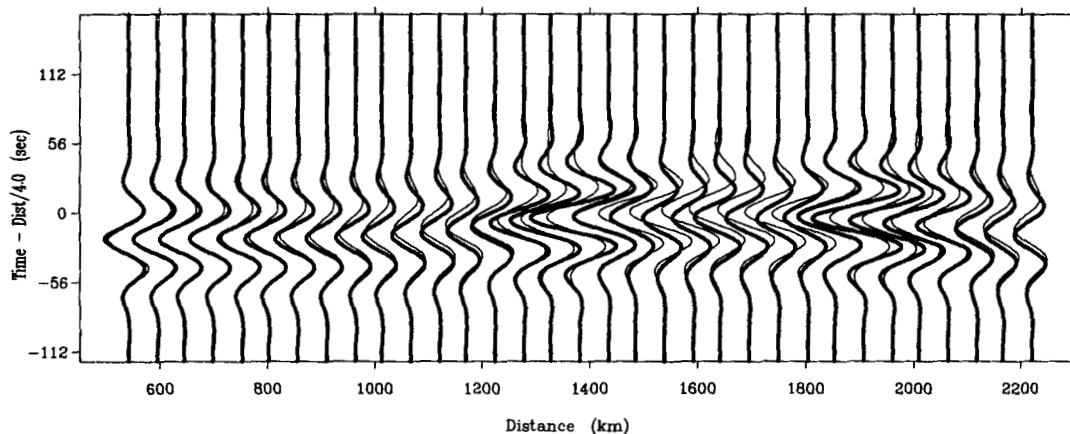


Figure 11. Narrow-band source, synthetic FD seismograms (thin lines) and WA seismograms (thick lines) for the 'deterministic' model and receiver locations shown in Fig. 10.

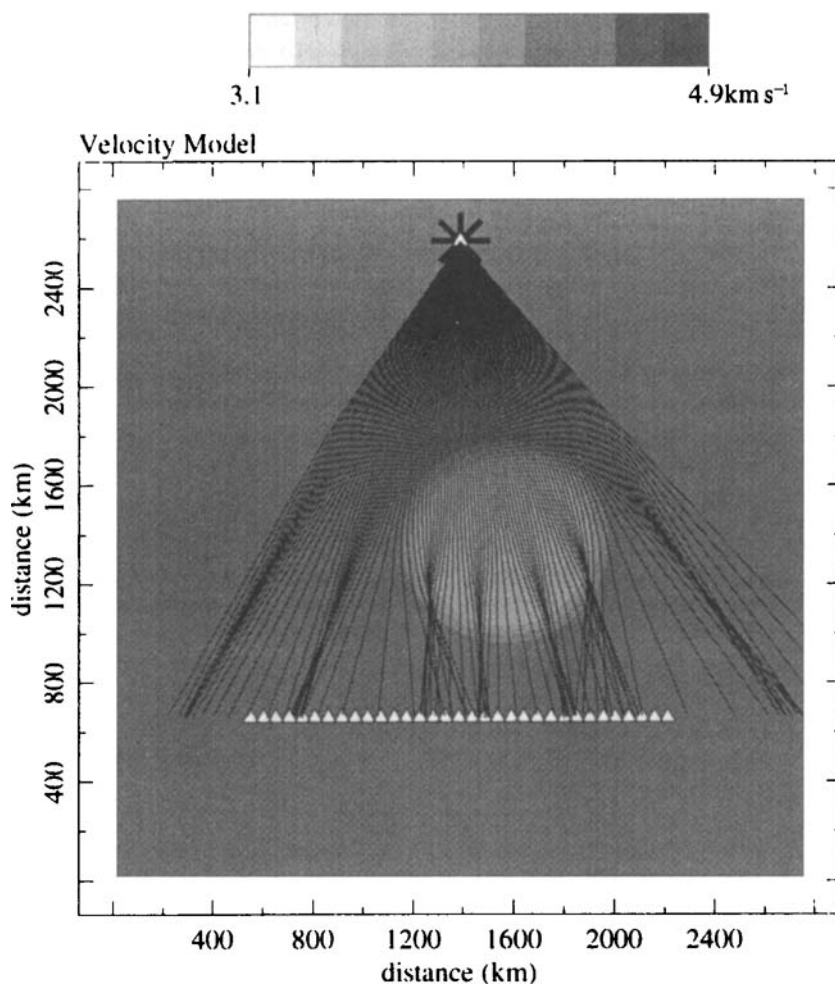


Figure 12. Wavelength-averaging wave paths at  $T_0 = 50$  s for the 'deterministic' model in Fig. 10.

reproduce the phase of the first-arriving energy better than the ray theory synthetics do (*cf.* Figs 6 and 9), which indicates that the WA method may be including some finite-frequency wave effects due to the medium properties away from the ray path.

### 4.3 Deterministic models

Next we compare FD and WA results for the narrow-band source ( $T_0 = 50$  s) in a 'deterministic' model composed of a low-velocity disc separated from a higher-velocity background

by a smooth transition over about a wavelength; the velocity change between the disc and background is about 10 per cent. Fig. (10) shows the velocity model and wave propagation for the FD simulation. Fig. (11) shows the FD and WA synthetic seismograms for the locations indicated in Fig. (10). The WA results follow the form of the FD synthetics, but there is not as good a match as with the 'quasi-random' model. This is most obvious in the region where the wavefield is most perturbed by the low-velocity disc (about  $1000 < \Delta < 2200$  km). The WA synthetics show a slight overestimate of amplitude at about  $\Delta \sim 1300$  km and  $\Delta \sim 1950$  km; the WA wave paths in these regions have passed close to and nearly tangent to the boundary of the disc (Fig. 12). At locations between these regions (about  $1400 < \Delta < 1900$  km), the WA seismograms slightly underestimate the amplitude and do not reproduce the complete phase delay of the FD synthetics. In addition, if the width of the velocity transition between the disc and background is decreased to less than a wavelength, the mismatch become more severe. These errors in the phase and amplitude estimates may be due to the interaction of the alternating positive and negative lobes of the weighting functions with the relatively sharp velocity transition in this model which leads to oscillating wave paths (Fig. 12).

Despite these shortcomings, the WA synthetics still show significant improvement over synthetics obtained from simple ray theory. Fig. (13) shows ray synthetics using the simple amplitude estimate based on the separation between ray paths. These ray synthetics show significant amplitude instability at caustics in the ray field near  $\Delta = 1400$  km and  $\Delta = 1950$  km; in these regions the WA synthetics show only a slight overestimate of amplitude (Fig. 11). Also, at the edge of the geometrical 'shadow' of the low-velocity disc (about  $\Delta = 900$  km) the ray synthetics show an abrupt change in amplitude that is not present in the FD or WA synthetics.

## 5 DISCUSSION

In Lomax (1994) a centrally peaked, non-oscillatory weighting function was shown to produce useful results in the wavelength-smoothing (WS) formulation in models with strong velocity differences across sharp boundaries. However, these weighting functions were not obtained through a theoretical development. In the present work we use a plane-wave construction and

single scattering to obtain theoretically derived weighting functions which are oscillatory and complex. These functions lead to the wavelength-averaging (WA) method, which produces useful finite-frequency seismograms in velocity structures with strong velocity variation, but which requires some restriction on the scale-length and extent of velocity variation relative to a wavelength. In particular, the new weighting functions do not give as good results in models with extensive regions of slowly varying velocity that are separated by strong gradients ('deterministic' models) as in models with more complex but smoothly varying velocity variations ('quasi-random' models). This limits application of the current formulation of the WA method to predominantly quasi-random structures, although such models may be useful in many problems, particularly for Monte-Carlo-based inversion methods requiring fast forward calculations.

A strength of the original WS algorithm (Lomax 1994) was the smoothing of features with small size relative to a wavelength, as this led to stability of wave paths at larger periods in complicated structures. The oscillating weighting functions in the current formulation give generally less stable wave paths, particularly if the velocity variation has a scale-length similar to the width of the lobes in the oscillating weighting functions. This may be understood as a change from tracking mainly the forward propagation of the wavefield in the original WS formulation, to tracking forward or scattered parts of the wavefield, depending on the details of the structure and wave path, in the new formulation. Further work is needed to investigate whether non-oscillatory weighting functions can be obtained from the theoretical development, or, alternatively, if the oscillating wave functions can be used in a manner that emphasizes the forward propagation of the wavefield and produces stable wave paths. This may require re-examination of the construction or application of eqs (16) and (17) for combining the incident and scattered fields in the thin slab approximation (Section 2.2).

## 6 ACKNOWLEDGMENTS

We thank Henk Marquering for providing the finite-difference code used in this work and we appreciate the extensive and helpful comments of the reviewers. This research was supported by the Netherlands Organization for Scientific

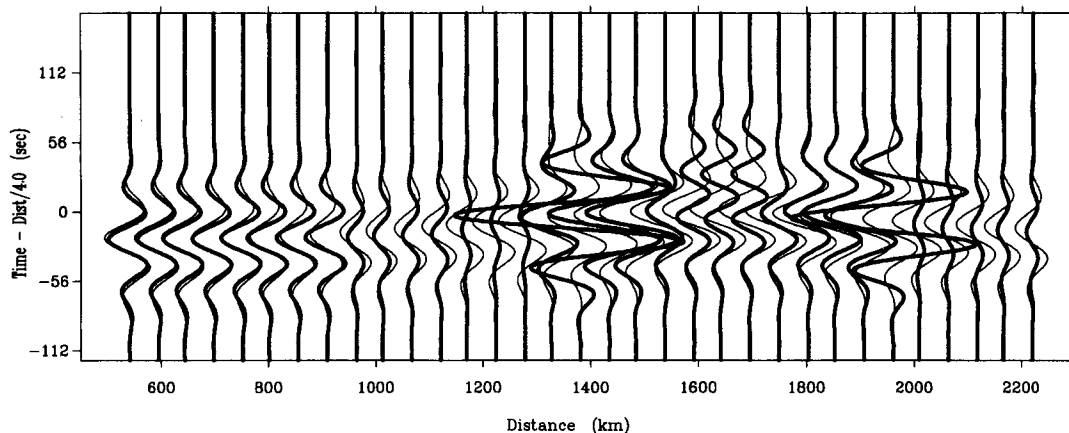


**Figure 13.** Simple ray-theory synthetic seismograms (thick lines) and FD seismograms (thin lines) for the 'deterministic' model and receiver locations shown in Fig. 10.

Research (NWO) through the Pionier project PGS 76-144. This is Geodynamics Research Institute (Utrecht University) publication 96.021.

#### REFERENCES

- Aki, K. & Richards, P.G., 1980. *Quantitative Seismology: Theory and Methods*, W.H. Freeman, San Francisco, CA.
- Hudson, J.A. & Heritage, J.R., 1982. The use of the Born approximation in seismic scattering problems, *Geophys. J. R. astr. Soc.*, **66**, 221–240.
- Kravtsov, Y.A. & Orlov, Y.I., 1993. *Caustics, Catastrophes and Wave Fields*, Springer Ser. Wave Phenom., Vol. 15, Springer, Berlin.
- Lomax, A., 1994. The wavelength-smoothing method for approximating broad-band wave propagation through complicated velocity structures, *Geophys. J. Int.*, **117**, 313–334.
- Morse, P. & Feshbach, H., 1953. *Methods of Theoretical Physics, Part I*, McGraw-Hill, New York, NY.
- Snieder, R. & Lomax, A., 1996. Wavefield smoothing and the effect of rough velocity perturbations on arrival times and amplitudes, *Geophys. J. Int.*, **125**, 796–812.